



LEIDENFROST DROPS

Benjamin Sobac^{1,3}, Alexey Rednikov¹, Stéphane Dorbolo² and Pierre Colinet¹

¹Université Libre de Bruxelles—TIPs Fluid Physics, Brussels, Belgium,

²Université de Liège—GRASP Laboratory, Liège, Belgium, ³Mechanical Engineering Department, Aix-Marseille University, Marseille, France

This chapter is concerned with drop levitation on a vapor layer when a volatile liquid is brought into contact with a very hot solid. This phenomenon is known as the Leidenfrost effect. A simple theory of a Leidenfrost drop covering the full range of stable shapes—that is, from small quasi-spherical droplets to larger puddles floating on a pocket-like vapor film—is presented. This modeling permits an accurate description of the geometry of the drop and of the underlying vapor film. It also provides deeper insights into heat transfer, evaporation, and flow that develop inside the vapor cushion. Finally, the model presented here can serve as a basis for studying other aspects or recent discoveries related to Leidenfrost drops. For instance, using a complement to the basic model, we show how to predict the lifetime of Leidenfrost drops.

7.1 Introduction

In 1756, Johann Gottlob Leidenfrost, a German physician, reported in his *Treatise on the Properties of Common Water* (Leidenfrost, 1756), “At the instant when the drop touches the glowing iron, it is spherical. It does not adhere to the spoon, as water is accustomed to do, which touches colder iron.” He further added that when he placed

a candle behind the drop, he could see light passing between the drop and the hot solid, revealing the existence of a vapor layer under the drop. Leidenfrost was probably not the first observer of this phenomenon, but he was the first to document it in detail. Therefore, the phenomenon bears his name. [Figure 7.1A](#) illustrates Leidenfrost's observation. A millimetric water drop "levitates" over a metallic substrate at 300°C. A small gap is indeed visible between the drop and the solid surface.

Indeed, a liquid that is placed on a solid surface at a temperature sufficiently above the saturation temperature does not come to a boil but rather levitates over a thin layer of its own vapor. The pressure exerted by the vapor emanating from the drop is able to sustain the weight of the drop. This levitation has mainly two consequences. First, the vapor layer preventing contact between the liquid and the heated surface ensures a higher degree of thermal insulation, conferring large lifetime to these objects. Second, this nearly frictionless state provides an extreme mobility to the drop, making it easy to manipulate but difficult to immobilize.

The Leidenfrost effect has been intensively investigated in the past ([Bernardin and Mudawar, 1999](#); [Biance et al., 2003](#); [Quééré, 2013](#)). However, many questions still remain open or under debate, in particular as far as the modeling of the phenomenon is concerned. A theoretical prediction of the Leidenfrost temperature is still unknown. This transition point depends on the nature of the liquid, as well as on the substrate's properties, such as surface roughness, thermal properties, and so on ([Bernardin and Mudawar, 1999](#)). Most experimental studies have concluded that the Leidenfrost temperature increases with the degree of roughness, the latter being detrimental to the stability of the vapor film. Accordingly, the generally accepted idea is that the higher the thermal diffusivity of the substrate and the smoother its surface ([Bernardin and Mudawar, 1999](#)), the closer the Leidenfrost point is to the saturation (boiling) temperature. However, a recent study also highlighted that a micropatterned surface can significantly reduce the Leidenfrost point ([del Cerro et al., 2012](#)). No present-day theory is able to explain these effects to the best of our knowledge.

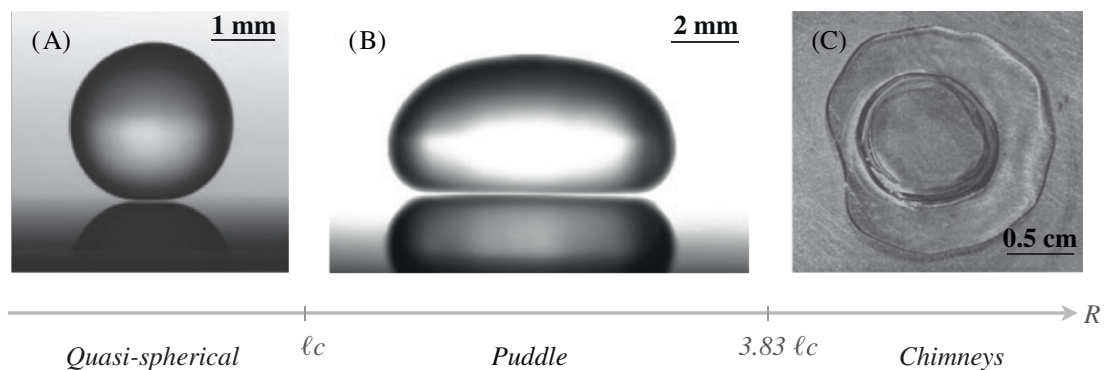


FIGURE 7.1 Typical shapes of Leidenfrost water drops of various sizes. A flat metallic substrate is maintained at 300°C. (A) and (B) Side view, courtesy of R. Thévenin and D. Soto. (C) Top view, taken from [Biance et al. \(2003\)](#), courtesy of A.-L. Biance.

The understanding and an accurate modeling of the Leidenfrost phenomenon are therefore crucial. Such a “film boiling” regime plays an important role in cooling devices. Indeed, if a vapor layer is present between the liquid and the device to be cooled, the energy transfer is drastically reduced, and the cooling becomes inefficient. This effect is, for example, undesirable from the point of view of rapid cooling of overheated components in high-power-density systems, such as nuclear reactors during possible accidents. On the other hand, the extreme mobility of the Leidenfrost drops and their nonwetting-like behavior make it possible to manipulate liquid mixtures without contact with any solid. This is a major advantage compared with regular micro- or millifluidic systems, where contact with walls is a potential source of pollution.

Recently, the Leidenfrost effect has been subject to a renewed interest following the discovery by [Linke et al. \(2006\)](#). Placed on an asymmetrically structured surface (called a ratchet), Leidenfrost drops can self-propel in a preferential direction with velocities of the order of 10 cm s^{-1} . These findings opened new doors to the control and manipulation of drops. It can indeed be particularly useful in systems where drops need to be transported rapidly and accurately. Playing on the geometry of the structure, it is then possible to control their velocities and trajectories and even to immobilize them ([Ok et al., 2011](#); [Cousins et al., 2012](#)). Taking advantage of this new control, such drops could, for example, be used to transport a component. Leidenfrost drops in mixtures is addressed in Chapter 24, but here, we discuss pure liquids.

This chapter is not intended to be a review of the subject. For a wider overview, the reader is referred to the recent review by [Qu  r   \(2013\)](#). Here, we concentrate on a recent model of a Leidenfrost drop. We use a simple theory that permits an accurate description of the geometry of the drop and the underlying vapor layer ([Sobac et al., 2014](#)). Because the evaporation of Leidenfrost drops is typically long compared to thermal and viscous relaxation times, only (quasi-) steady shapes are considered. This modeling appears to nicely match experimental data and in particular provides a good picture of the influence of the superheat and drop size on the Leidenfrost drop geometry. Moreover, it gives us deeper insights into the heat transfer, evaporation, and flow developing inside the vapor cushion. Finally, we show that the modeling can be extended to predict the lifetime of Leidenfrost drops and is readily amenable to further generalization.

7.2 Shape of Leidenfrost drops

Because there is no contact between the Leidenfrost drop and the surface, the apparent contact angle is 180° . A Leidenfrost drop therefore resembles a perfect superhydrophobic drop. [Figure 7.1](#) shows the various shapes that a Leidenfrost

drop can adopt, depending on its size. The smaller drops are quasi-spherical (Figure 7.1A), whereas the larger ones are flattened by gravity (Figure 7.1B). This transition between the spheres and puddles occurs when the gravity forces overcome the capillary ones. Typically, the effect of gravity on the drop shape can be disregarded when the drop radius R (as seen from the top of the drop) is smaller than the capillary length $\ell_c = (\gamma/\rho_\ell g)^{1/2}$, where g , γ , and ρ_ℓ are the gravity acceleration, surface tension, and liquid density, respectively. In a Leidenfrost situation, the temperature inside the drop is at the saturation (boiling) temperature (Biance et al., 2003). For water, this implies a density $\rho_\ell = 960 \text{ kg m}^{-3}$ and a surface tension $\gamma = 59 \text{ mN m}^{-1}$, and thus a capillary length $\ell_c = 2.5 \text{ mm}$. When the size of the drop is too large, the shape of the drop becomes unstable. The underlying vapor layer destabilizes, and vapor chimneys form, rising and eventually bursting through the center of the puddle (Figure 7.1C). This phenomenon has been interpreted as a Rayleigh–Taylor instability that develops as soon as $R > 4\ell_c$ (Biance et al., 2003; Snoeijer et al., 2009). Under certain conditions, drops spontaneously start to oscillate and develop “star shapes” or “faceted shapes” (Brunet and Snoeijer, 2011). The model presented here is limited to axisymmetric stable shapes of Leidenfrost drops—that is, to $R < 4\ell_c$.

7.2.1 EQUILIBRIUM DROP SHAPE (OUTER DROP SURFACE)

The upper part of the drop, above the vapor cushion, is assumed to be of equilibrium shape. At equilibrium, the Laplace pressure $\gamma\kappa$ (with κ the curvature of the drop surface) balances (up to a constant) the hydrostatic pressure $-\rho_\ell g z$, where z is the vertical coordinate directed upward. Scaling all lengths by ℓ_c and counting z from the top of the drop, the dimensionless equation for the equilibrium shape then simply reads

$$\kappa + z = \kappa_{\text{top}} \quad (7.1)$$

where κ_{top} is the curvature at the top of the drop. Numerically integrating this differential equation for a given value of κ_{top} yields equilibrium shapes and in particular the value of the radius $R = R(\kappa_{\text{top}})$. The integration can be continued up to a horizontal local slope, beyond the envisaged applicability of an equilibrium shape, yielding the associated superhydrophobic drop (whose upper part coincides with that of our Leidenfrost shape); see Figure 7.2. The height and the contact radius of this superhydrophobic drop are $H = H(\kappa_{\text{top}})$ and $R_c = R_c(\kappa_{\text{top}})$, respectively. The height varies from $H \approx 2R$ for small drops (which are quasi-spherical, with the curvature $\kappa_{\text{top}} \approx 2/R$) to $H \approx 2.1$ for large drops (the top of the puddle being almost flat, the curvature $\kappa_{\text{top}} \approx 0$). Note also that in the limit $R \ll 1$, the contact radius is given by $R_c = \sqrt{2/3} R^2$ (Mahadevan and Pomeau, 1999; Burton et al., 2012), whereas in the limit of $R \gg 1$, R_c scales as R .

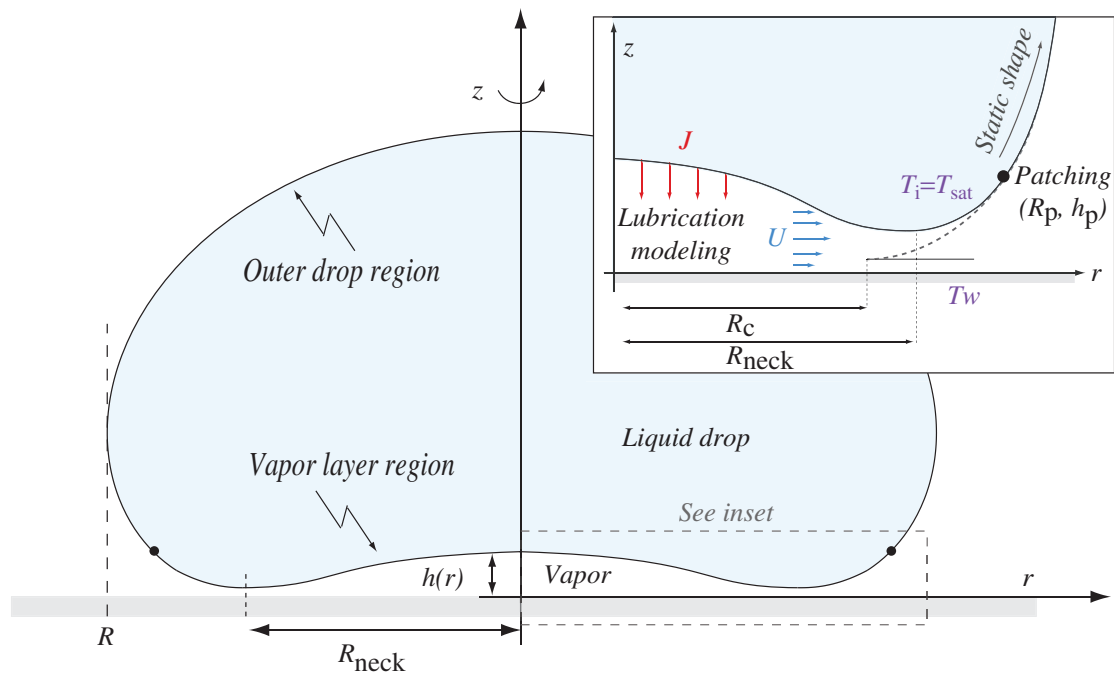


FIGURE 7.2 Schematic illustration of a Leidenfrost drop. The drop levitates on a vapor cushion of nonuniform thickness profile $h(r)$, composed by a pocket surrounded by an annular neck. Due to evaporation, an outward radial flow develops in the vapor layer. R is the drop radius as seen from above, while R_{neck} is the radius of the neck (at its thinnest section). The outer drop region (assumed to be an equilibrium shape) and the inner vapor layer region (described using lubrication theory, including evaporation) are solved separately and numerically matched at the “patching” point with coordinates (R_p, h_p) . R_c is defined from the outer drop shape as the “contact” radius of the associated superhydrophobic drop at equilibrium.

In the case of a Leidenfrost state, however, the drop does not contact the substrate but rather levitates on a vapor cushion. It is unlikely that the bottom remains flat, especially for $R > 1$ when gravity becomes stronger than capillarity. Indeed, we then rather expect the formation of a vapor pocket below the drop similarly to what happens in film boiling regimes. In the framework of our model of the Leidenfrost drop, the equilibrium shape is applied only until a point located at $r = R_p$, between R_c and R (Figure 7.2), where nonequilibrium effects of evaporation and viscous pressure losses in the underlying vapor layer come into play. Let us now discuss the shape of the liquid/vapor interface under the drop.

7.2.2 VAPOR FILM GEOMETRY

In the vapor layer region ($0 < r < R_p$), the gas is assumed to be pure vapor and incompressible, and its properties are taken as constant. Assuming that heat is only transferred by conduction across the film, the local evaporation flux at the

interface is expressed as $J = L^{-1}\lambda_v(T_w - T_i)/h$, where λ_v is the vapor thermal conductivity, T_i is the liquid–vapor interface temperature equal to the saturation temperature T_{sat} , T_w is the substrate temperature, and L is the latent heat of vaporization. The drop squeezing the vapor exerts an excess of pressure P_v , forcing the vapor to escape laterally. Ignoring possible motion inside the drop as it is typically the case in the literature (Snoeijer et al., 2009), the balance of normal forces at the drop interface gives $P_v = -(\rho_\ell gh + \gamma\kappa)$ up to a constant. The thickness of the vapor film and its slope can be considered small enough so as to use the lubrication approximation. Then, this pressure drives a Poiseuille flow with a volumetric flux $\vec{q} = -\frac{h^3}{12\mu_v}\vec{\nabla}P_v$, where μ_v is the vapor dynamic viscosity. Note the coefficient 1/12 in the mobility factor, typical of no-slip conditions imposed both at the drop surface and at the substrate. Finally, the classical expression of vapor mass conservation under the lubrication hypothesis (at steady state) reads $\vec{\nabla}\cdot\vec{q} - J/\rho_v = 0$, where ρ_v is the vapor density. Combining these equations, scaling all lengths by ℓ_c , and assuming the axial symmetry yields the following equation for the film thickness:

$$\frac{1}{12} \frac{1}{r} \frac{\partial}{\partial r} \left(rh^3 \frac{\partial}{\partial r} (h + \kappa) \right) - \frac{E}{h} = 0 \quad (7.2)$$

with an evaporation number E defined by

$$E = \frac{\lambda_v \mu_v \Delta T}{\gamma \rho_v \ell_c L} \quad (7.3)$$

where $\Delta T = T_w - T_{\text{sat}}$ is the superheat. As for the curvature κ , it is here taken in a general form

$$\kappa = \frac{\frac{\partial^2 h}{\partial r^2} + \frac{1}{r} \left[1 + \left(\frac{\partial h}{\partial r} \right)^2 \right] \frac{\partial h}{\partial r}}{\left[1 + \left(\frac{\partial h}{\partial r} \right)^2 \right]^{3/2}} \quad (7.4)$$

It is interesting to note that E is hereby the only parameter remaining in the problem, apart from the size R of the drop, and depends on the fluid properties and the superheat ΔT . While the liquid properties are taken at T_{sat} , the vapor properties are here evaluated at the mean temperature $(T_w + T_{\text{sat}})/2$ of the vapor film and thus they vary with the substrate temperature. Four boundary conditions are needed to solve Eqs (7.2) and (7.4): symmetry conditions at $r = 0$ —that is, $h'(0) = 0$ and $\kappa'(0) = 0$ —while at $r = R_p$ the solution must match with the outer equilibrium shape of the drop—that is, the continuities of $h'(r)$ and $\kappa(r)$ are required. The continuity of $h(r)$ itself here merely amounts to a vertical shift of the outer shape. This problem is numerically solved using a standard second-order finite-difference method, and it is checked a posteriori that the choice of the “patching” point R_p has an insignificant influence on the results (up to a few percent).

Figure 7.3 shows typical shapes of Leidenfrost drops computed with the present model for various drop sizes. It is seen that the vapor layer forms a concave depression in the drop interface that becomes increasingly marked with the drop size. The vapor layer is composed of a vapor pocket at its center, surrounded by an annular neck. The film thickness at the neck location appears to increase with the drop size at a given E (inset of Figure 7.3). Figures 7.4A–C describe the Leidenfrost drop shape by means of the values of the neck thickness h_{neck} , the depth of the vapor pocket $\Delta h = h_{\text{center}} - h_{\text{neck}}$, and the neck radius R_{neck} as a function of the drop size. It can be seen that the vapor cushion thickness increases with the drop size. In the situation where $E = 7.16 \times 10^{-7}$ (i.e., a water drop on a substrate at $T_w = 300^\circ\text{C}$), the neck thickness can reach $60 \mu\text{m}$ for puddles. The drop bottom is almost flat $\Delta h \approx 0$ for small drops, but the depth of the vapor pocket strongly increases with the drop size ($\Delta h \sim H$ when $R \approx 3.9$). Finally, the neck radius R_{neck} increases linearly with R when $R > 1$. Recently, Burton et al. (2012) experimentally studied the bottom of Leidenfrost drops by observing water drops on a hot transparent surface from below. Then, using interferometry, they characterized the shape of the vapor layer for various drop sizes and substrate temperatures. A comparison between these experimental data and the present model showed a good agreement (Sobac et al., 2014). It appears, among other things, that the position of the neck practically does not depend on the superheat and that the geometry of the vapor layer is much more affected by the drop size than by the applied superheat (Figure 7.4). The influence of the evaporation number on the vapor cushion characteristics is reported in Figures 7.4D and E. While the neck thickness turns out to scale as $h_{\text{neck}} \sim E^{1/3}$ for all the drop sizes considered in the figure, the pocket thickness grows more slowly as $h_{\text{center}} \sim E^{1/6}$, except for sufficiently small droplets, where the pocket levels with the neck and the exponent gets larger (closer to $1/3$). The superheat value thus appears to have a more appreciable effect on the film in the neck region. These scalings can be directly obtained from Eq. (7.2) by an asymptotic

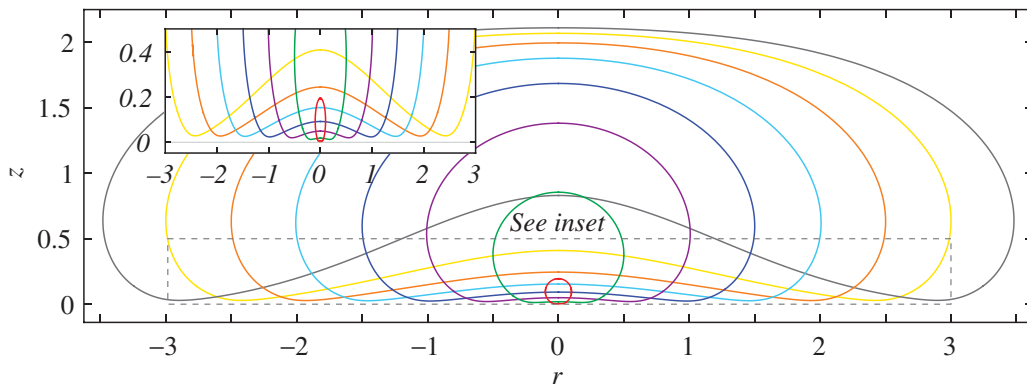


FIGURE 7.3 Numerically determined shapes of Leidenfrost drops for an evaporation number $E = 1.21 \times 10^{-6}$ ($T_w = 370^\circ\text{C}$ for water). The lengths are scaled by the capillary length (i.e., 2.5 mm for water).

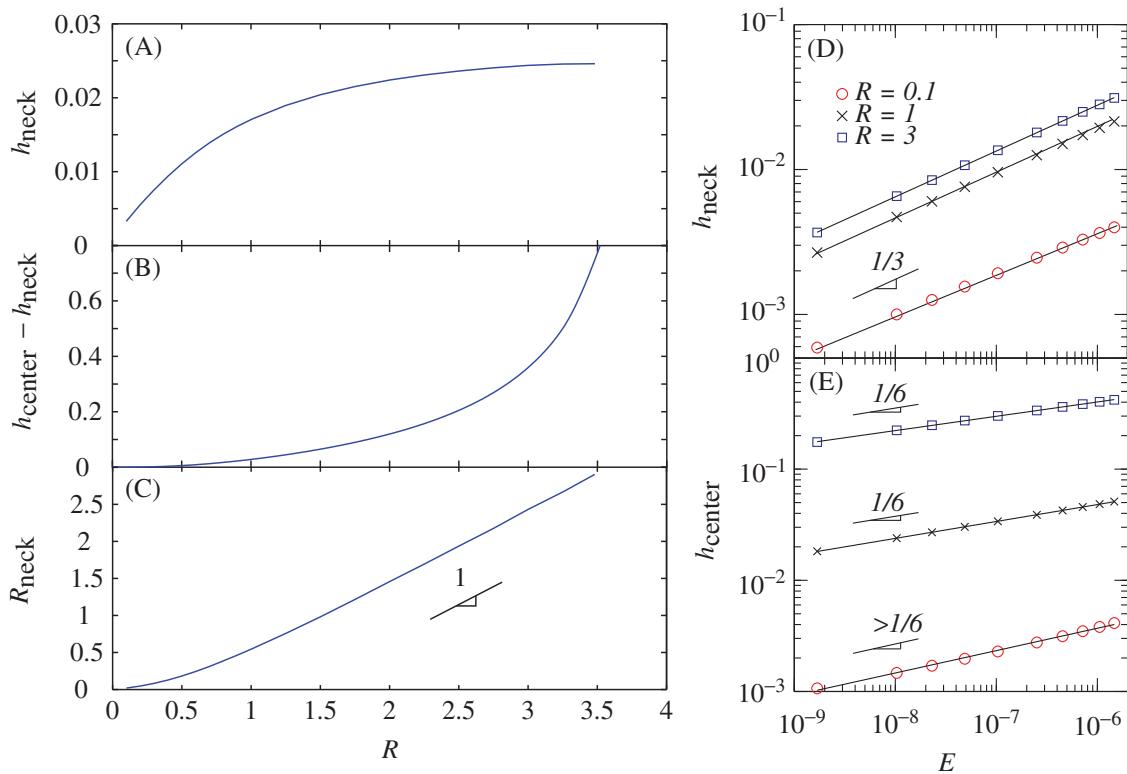


FIGURE 7.4 Geometrical parameters of the vapor layer under a Leidenfrost water drop over a substrate at $T_w = 300^\circ\text{C}$ (i.e., $E = 7.16 \times 10^{-7}$). Neck thickness (A), depth of the vapor pocket (B), and neck radius (C) are plotted as a function of the drop size. All lengths are scaled by the capillary length $\ell_c = 2.5$ mm. The neck thickness (D) and the vapor-film thickness in the center (E) are also plotted versus the evaporation number for some drop sizes.

analysis on account of E being small (see Sobac et al., 2014). A slightly different scaling exponent for h_{center} was proposed by Pomeau et al. (2012) (although these authors also find $h_{\text{neck}} \sim \Delta T^{1/3}$)—namely, $1/5$ was obtained instead of $1/6$, against which we argued elsewhere (Sobac et al., 2014). We will see in the following section that this result is related to a rather important conceptual difference concerning the physics of the vapor layer. Understanding the shape and physical mechanisms at play in the film is crucial to predicting the heat transfer between the solid and the liquid, a practically important quantity, as well as the global evaporation rate of the drop or the drop lifetime (see Section 7.4).

7.3 Physics of the vapor film

In this section we look more closely at the physical mechanisms at play inside the vapor layer. It has already been mentioned that radial Poiseuille flow is driven in the vapor film underneath the drop. Given the no-slip conditions both

at the plate and the interface, the maximum vapor velocity at a given radial location is thus located in the middle of the vapor layer, at $z = h/2$. **Figure 7.5A** shows the radial profile of this velocity U_{\max} for various sizes of the drop. It is worth mentioning that U_{\max} can attain values of the order of several meters per second in the vicinity of the neck (where U_{\max} reaches its maximum, denoted as U_{neck} , even though it may not be exactly at the neck itself). The velocity difference between the pocket and the neck regions is more pronounced for puddles. Moreover, the magnitude of the velocity decreases with the increase in the drop size, the effect being apparently determined by the associated increase in the layer thickness. The local Reynolds number in the neck region, defined as $\text{Re} = \rho_v U_{\text{neck}} h_{\text{neck}}^2 / \mu_v \ell_{\text{neck}}$ and comparing the inertial and viscous effects therein, is then found to be of the order of 0.1 (inset of **Figure 7.5A**). This justifies a

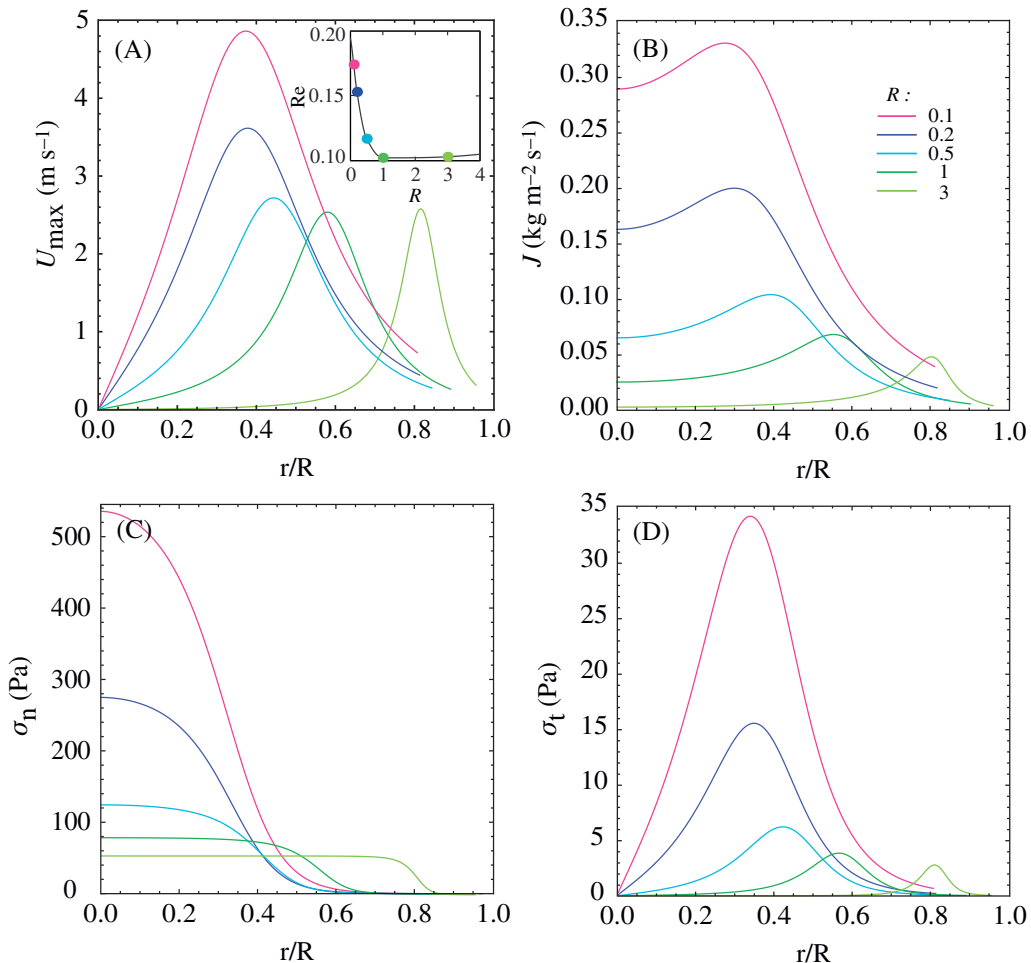


FIGURE 7.5 Some relevant flow quantities inside the vapor layer underneath a Leidenfrost water drop, the substrate being at $T_w = 300^\circ\text{C}$ (i.e., $E = 7.16 \times 10^{-7}$). Radial profile of the maximum local velocity (A), the local evaporation flux (B), and the (excess) normal (C) and tangential (D) stresses acting on the bottom surface of the drop for various drop sizes. The profiles end at the patching points.

posteriori the dominant role of viscous forces in the vapor film assumed in the present analysis. Here, ℓ_{neck} is the length of the neck region as it appears at the height $2h_{\text{neck}}$ of the film profile.

Similar observations can be made for the profile of the local evaporation flux J (Figure 7.5B). Considering conduction in the vapor as the main mechanism of heat exchange between the substrate and the drop, the profile of J scales as $1/h$. Evaporation is thus more intense in the neck region, and an appreciable effect of evaporation on the film geometry in this place is not surprising. On the contrary, it turns out that the shape of the central pocket is almost unaffected by evaporation (it is an equilibrium shape governed by capillarity and gravity, just like the top of the drop (Sobac et al., 2014)). This contrasts with the analysis of Pomeau et al. (2012), who (unrightfully in our opinion) assumed that evaporation affects the shape of the vapor pocket already to the same order of magnitude as gravity and capillarity (see Sobac et al., 2014; it is also the basis of the earlier mentioned different scaling for h_{center} obtained in Pomeau et al., 2012). The Péclet number $Pe = Pr Re$ (where $Pr = \nu_v/\alpha_v \sim 0.7$ is the Prandtl number, and α_v is the thermal diffusivity of vapor) comparing heat transfer by convection and conduction is estimated to be of the order of 0.1, as well, supporting a posteriori the hypothesis of a mostly conductive heat transfer in the vapor film. A scaling argument reveals that the dimensionless rate of vapor production over the pocket is of the order of $(E/h_{\text{center}})\pi R_{\text{neck}}^2 \sim E^{5/6}$ where $\ell_{\text{neck}} \sim E^{1/6}$ and $R \sim 1$, which is comparable to the global evaporation rate in the neck region $(E/h_{\text{neck}})2\pi\ell_{\text{neck}}R_{\text{neck}} \sim E^{5/6}$ (Sobac et al., 2014). Thus, even though the local rate of evaporation is much lower in the pocket region than in the neck, it occurs on a larger surface, so that both regions contribute by the same order of magnitude to the global evaporation rate. Note that the conclusions of Pomeau et al. (2012) also differ from ours in that respect; that is, unlike the present study, they found that the global evaporation rate is mainly determined by the pocket region.

Finally, Figures 7.5C and D present the tangential and (excess) normal stresses acting on the drop. The normal stresses sustain the levitation of the drop and are (in the lubrication approximation) equal to the vapor pressure, for which we here plot the excess value (relative to the ambient one). These stresses are maximum in the vapor pocket and quickly vanish through the neck region. Furthermore, they are quite homogeneous in the pocket underneath large puddles. The integral of the excess normal stresses over the bottom surface of the drop must be equal to the weight of the drop, which has been verified numerically. Note that these excess normal stresses in the vapor film underneath the drops can be as large as 5×10^{-3} atm. The values of the tangential (viscous) stresses $\sigma_t = \mu_v \partial u / \partial z|_{z=h}$ are about an order of magnitude smaller. These tangential stresses are obviously most important in the neck region. Needless to say, the integral of these tangential viscous stresses over the bottom surface of the drop is equal to zero by symmetry, which is compatible with the drop remaining static.

7.4 Global evaporation rate and lifetime

An integration of the local evaporation flux J all over the drop surface allows us to evaluate the quantity of vapor produced per unit time ($-\dot{M}$, the global evaporation rate). The model developed thus far yields us right away the global evaporation rate in the underlying film (from $r = 0$ to $r = R_p$): $(-\dot{M}_{\text{film}}) = \frac{2\pi\lambda_v\Delta T}{L} \int_0^{R_p} r \frac{dr}{h}$. This evaporation rate is typically of the order of 1 mg s^{-1} , and it depends on the size of the drop. We can now numerically confirm the scaling we obtained before that shows that the effects of the vapor pocket and neck regions on the overall evaporation rate are of the same order of magnitude. Even though evaporation also occurs on the rest of the drop surface, $(-\dot{M}_{\text{film}})$ should be the main contribution into $(-\dot{M})$ in view of the thinness of the film. Nonetheless, we shall here be interested in accounting for evaporation over the entire surface of the drop. To this purpose, the following simplified approach is used. Having already obtained the overall Leidenfrost drop geometry in the framework of our model, we can now simply solve the stationary heat transfer problem for this fixed geometry. In principle, if the convective (maybe including buoyancy) contribution is important, it should also include a resolution of the Navier–Stokes equations in conjunction with the energy equation. In this chapter, however, we limit ourselves to the case of pure conduction when the gas temperature field T_g satisfies just the Laplace equation $\nabla^2 T_g = 0$. The drop is still assumed to be at the boiling temperature—that is, $T_g = T_{\text{sat}}$ at the drop surface. At the substrate, we still have $T_g = T_w$. As for the ambient temperature, we assume that the vicinity of the drop is heated up to the temperature of the substrate, hence $T_\infty = T_w$ for the temperature that is formally imposed for T_g at infinity. The formulated problem for T_g (which is 2D axisymmetric) is here solved using the COMSOL Multiphysics™ software. The local evaporation rate at the drop surface is then calculated as $J = \frac{\lambda_v}{L} \frac{\partial T_g}{\partial n}$, whereas the global one is $(-\dot{M}) = \frac{\lambda_v}{L} \int \frac{\partial T_g}{\partial n} dS$, by integrating over the entire surface area of the drop, where n is the external normal. As before, λ_v is here evaluated at the “mean” vapor temperature—that is, $(T_w + T_{\text{sat}})/2$. The results for the gas temperature field and the local and global evaporation rates are shown in Figure 7.6. As previously observed in Figure 7.5B, the local evaporation rate increases from the center of the vapor pocket to reach a maximum at the neck. Then, the local evaporation rate decreases down to a minimum at the top of the drop. Evaporation is thus more intense in the neck region, as it has been previously pointed out. Evaporation at the top of the drop appears to be relatively weak compared to the contribution of the vapor layer. However, considering the global evaporation rate (Figure 7.6D), the contribution of the upper part (i.e. above the patching point) to the evaporation rate does not appear to be negligible, at least not for the small drops. Indeed, the inset in Figure 7.6D shows the quantity $((-\dot{M}) - (-\dot{M}_{\text{film}}))/(-\dot{M}) \equiv \varepsilon_{\dot{M}}$, which represents the relative contribution of the upper part of the drop into the global evaporation rate.

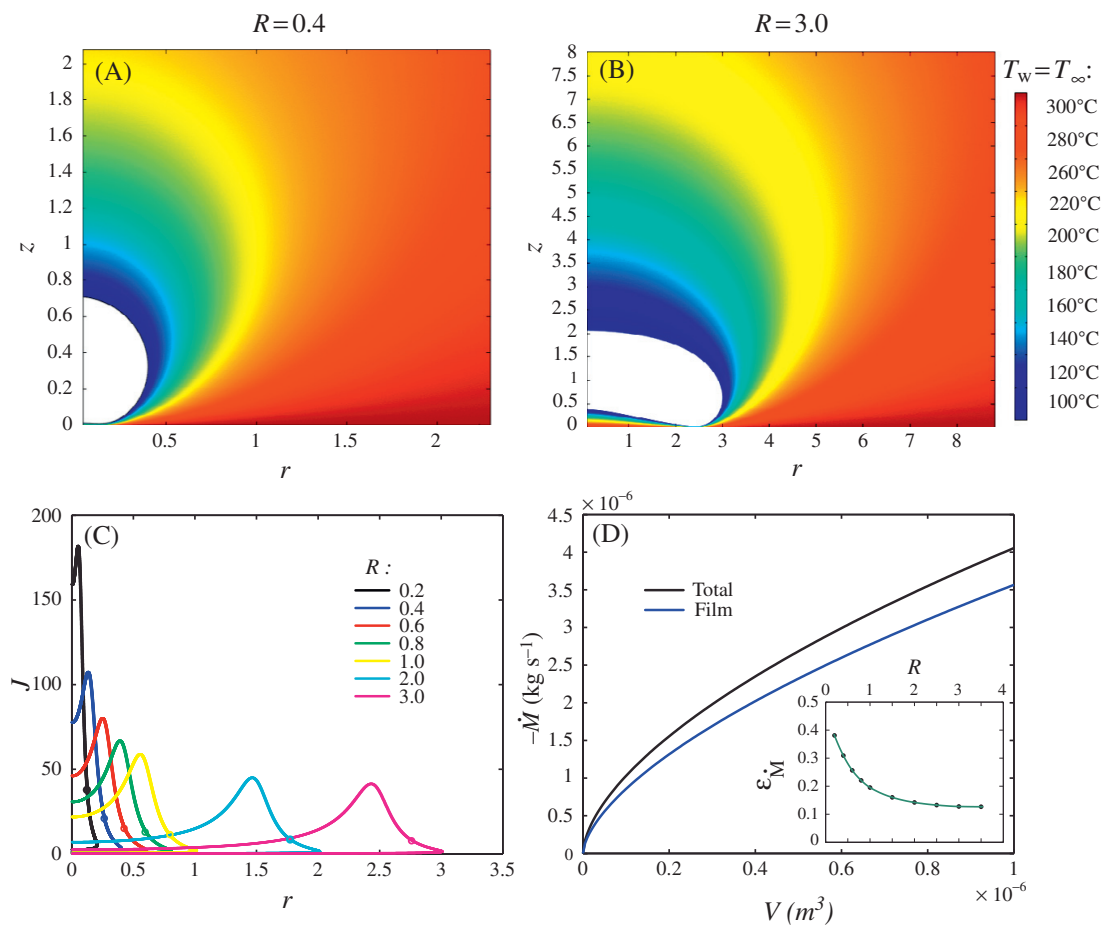


FIGURE 7.6 Evaporation of a Leidenfrost water drop over a surface at 300°C. (A and B) Temperature fields around drops of two different sizes ($R = 0.4$ and $R = 3.0$). (C) Dimensionless profile of the local evaporation flux at the drop surface for drops of various sizes (the open circles indicate the location of the patching points). (D) Global evaporation rate as a function of the drop volume, both the one obtained all over the drop surface and the one in the vapor film only. Inset: The relative difference between the two.

It reveals that for puddles ($R \gg 1$), the drop evaporates mainly via the vapor film; the upper part contributes only about 10% to drop evaporation. But this is not the case for smaller drops ($R \leq 1$), where evaporation takes place over the entire surface, rather than mostly in the film. The upper surface then contributes about 40% to drop evaporation with a dimensionless radius $R = 0.2$. These conclusions are found to be in qualitative agreement with the results of [Biance et al. \(2003\)](#). On the other hand, as it can be appreciated from [Figure 7.6C](#), a big part of the upper-surface contribution comes in fact from its lower part, between the point of patching and the turning point $r = R$. Note finally that the global evaporation rate \dot{M} turns out to scale approximately as $V^{0.6}$ ([Figure 7.7A](#)).

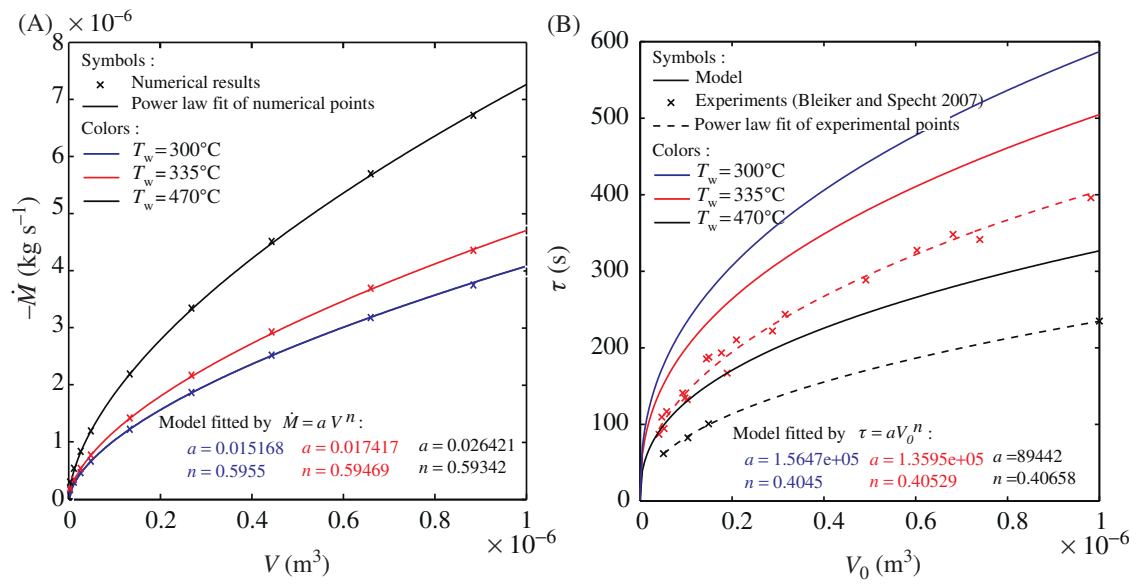


FIGURE 7.7 Global evaporation rate (A) and lifetime (B) of a water drop as a function of its size for several substrate temperatures. The predicted lifetime are compared with experimental data extracted from [Bleiker and Specht \(2007\)](#).

We can now estimate the lifetime of an evaporating Leidenfrost drop $\tau = \rho_\ell \int_0^{V_0} dV / -\dot{M}$, where V_0 is the initial drop volume. A water Leidenfrost puddle of a few millimeters ($V_0 = 0.1$ mL) evaporates over a substrate at 300°C in 230 s according to our prediction, including evaporation all around the drop. Assuming that the drop only evaporates through the film, we instead get a lifetime estimate of 295 s. This simplification clearly leads to an overestimation of the lifetime by about 30%. The smaller the drop, the higher the overestimation due to this assumption. Therefore, evaporation all around the drop appears crucial for a correct lifetime estimate, even for puddles. [Figure 7.7](#) shows the influence of the substrate temperature on the evaporation rate and on the lifetime of an evaporating Leidenfrost drop. The predicted evaporation times are compared to experimental data extracted from [Bleiker and Specht \(2007\)](#). The model prediction appears to overestimate the experimental lifetime of the drop. The overestimation is of the order of 25% for puddles over a substrate at 335°C and 38% over a substrate at 470°C . Part of this discrepancy is deemed to be due to convective effects, neglected in the present study, which would tend to increase the evaporation rate over the upper part of the droplet. On the other hand, the gas was here considered as pure vapor even all around the upper part of the drop which must not be exactly the case in experiments.

7.5 Conclusions and perspectives

The theory presented here provides an accurate description of the overall geometry of the Leidenfrost drop and of the underlying vapor layer, which proves to be composed of a vapor pocket at its center, surrounded by an annular neck. This enables us to examine the roles of heat transfer, evaporation, and flow developing inside the vapor layer. The model reveals in particular that the vapor flow developing in the film is dominated by viscous forces ($Re \ll 1$) and that the heat is mostly transferred by conduction ($Pe \ll 1$). Moreover, it turns out that evaporation has a more appreciable effect on the film geometry in the neck region and that the contributions of the pocket and neck regions to the global evaporation rate are comparable. This simple theory of the Leidenfrost effect can serve as a basis for further studies. For instance, it could be generalized to account for substrate non-flatness (roughness, geometrical structures), internal flow in the drop, and so on. As for this chapter, our basic model has in particular been supplemented with a consideration of the evaporation flux over the upper part of the drop, yielding the overall evaporation flux and permitting us to estimate the lifetime of the drop. The relative contribution of the upper part of the drop to the global evaporation rate reveals that for puddles ($R \gg \ell_c$), the drop evaporates mainly via the vapor film (pocket and neck), whereas for smaller drops ($R \leq \ell_c$), evaporation takes place over the entire surface, rather than mostly in the film. However, examining the evaporation that occurs all around the drop is crucial for estimating the lifetime accurately, even for puddles, because this regime contributes more to the total evaporation time than the spherical drop regime.

References

- Bernardin, J.D., Mudawar, I., 1999. The Leidenfrost point: experimental study and assessment of existing models. *J. Heat Transf.* 121, 894–903.
- Biance, A.-L., Clanet, C., Quéré, D., 2003. Leidenfrost drops. *Phys. Fluids* 15 (6), 1632–1637.
- Bleiker, G., Specht, E., 2007. Film evaporation of drops of different shape above a horizontal plate. *Int. J. Therm. Sci.* 46, 835–841.
- Brunet, P., Snoeijer, J., 2011. Star-drops formed by periodic excitation and on an air cushion—a short review. *Eur. Phys. J. Special Topics* 192, 207–226.
- Burton, J.C., Sharpe, A.L., van der Veen, R.C.A., Franco, A., Nagel, S.R., 2012. Geometry of the vapor layer under a Leidenfrost drop. *Phys. Rev. Lett.* 109, 074301.
- Cousins, T.R., Goldstein, R.E., Jaworski, J.W., Pesci, I.A., 2012. A ratchet trap for Leidenfrost drops. *J. Fluid Mech.* 696, 215–227.
- del Cerro, D.A., Marín, A.G., Römer, G.R.B.E., Pathiraj, B., Lohse, D., Huis in't Veld, A.J., 2012. Leidenfrost point reduction on micropatterned metallic surfaces. *Langmuir* 28, 15106–15110.

- Leidenfrost, J.G., 1756. On the fixation of water in diverse fire (Trans. C. Wares, 1966). *Int. J. Heat Mass Transf.* 9, 1153–1166.
- Linke, H., Alemán, B., Melling, L., Taormina, M., Francis, M., Dow-Hygelund, C., Narayanan, V., Taylor, R.P., Stout, A., 2006. Self-propelled Leidenfrost droplets. *Phys. Rev. Lett.* 96 (15), 154502.
- Mahadevan, L., Pomeau, Y., 1999. Rolling droplets. *Phys. Fluids* 11, 2449–2453.
- Ok, J., Lopez-Ona, E., Nikitopoulos, D., Wong, H., Park, S., 2011. Propulsion of droplets on micro- and sub-micron ratchet surfaces in the Leidenfrost temperature regime. *Microfluid. Nanofluid.* 10, 1045–1054.
- Pomeau, Y., Le Berre, M., Celestini, F., Frisch, T., 2012. The Leidenfrost effect: from quasi-spherical droplets to puddles. *C. R. Mecanique* 340, 867–881.
- Quéré, D., 2013. Leidenfrost dynamics. *Ann. Rev. Fluid Mech.* 45, 197–215.
- Snoeijer, J., Brunet, P., Eggers, J., 2009. Maximum size of drops levitated by an air cushion. *Phys. Rev. E* 79, 036307.
- Sobac, B., Rednikov, A., Dorbolo, S., Colinet, P., 2014. Leidenfrost effect: accurate drop shape modeling and refined scaling laws. *Phys. Rev. E* 90, 053011.